A New Dual-Polarization Radar Rainfall Algorithm: Application in Colorado Precipitation Events

R. CIFELLI

National Oceanic and Atmospheric Administration/Earth System Research Laboratory, Boulder, and Cooperative Institute for Research in the Atmosphere, Colorado State University, Fort Collins, Colorado

V. CHANDRASEKAR AND S. LIM

Department of Computer and Electrical Engineering, Colorado State University, Fort Collins, Colorado

P. C. KENNEDY

Department of Atmospheric Science, Colorado State University, Fort Collins, Colorado

Y. WANG

Department of Computer and Electrical Engineering, Colorado State University, Fort Collins, Colorado

S. A. RUTLEDGE

Department of Atmospheric Science, Colorado State University, Fort Collins, Colorado

(Manuscript received 29 April 2010, in final form 8 November 2010)

ABSTRACT

The efficacy of dual-polarization radar for quantitative precipitation estimation (QPE) has been demonstrated in a number of previous studies. Specifically, rainfall retrievals using combinations of reflectivity (Z_h), differential reflectivity (Z_{dr}), and specific differential phase (K_{dp}) have advantages over traditional Z–R methods because more information about the drop size distribution (DSD) and hydrometeor type are available. In addition, dual-polarization-based rain-rate estimators can better account for the presence of ice in the sampling volume.

An important issue in dual-polarization rainfall estimation is determining which method to employ for a given set of polarimetric observables. For example, under what circumstances does differential phase information provide superior rain estimates relative to methods using reflectivity and differential reflectivity? At Colorado State University (CSU), an optimization algorithm has been developed and used for a number of years to estimate rainfall based on thresholds of Z_h, Z_{dr}, and K_{dp}. Although the algorithm has demonstrated robust performance in both tropical and midlatitude environments, results have shown that the retrieval is sensitive to the selection of the fixed thresholds.

In this study, a new rainfall algorithm is developed using hydrometeor identification (HID) to guide the choice of the particular rainfall estimation algorithm. A separate HID algorithm has been developed primarily to guide the rainfall application with the hydrometeor classes, namely, all rain, mixed precipitation, and all ice.

Both the data collected from the S-band Colorado State University–University of Chicago–Illinois State Water Survey (CSU–CHILL) radar and a network of rain gauges are used to evaluate the performance of the new algorithm in mixed rain and hail in Colorado. The evaluation is also performed using an algorithm similar to the one developed for the Joint Polarization Experiment (JPOLE). Results show that the new CSU HID-based algorithm provides good performance for the Colorado case studies presented here.

Corresponding author address: Robert Cifelli, R/PSD2, 325 Broadway, Boulder, CO 80305.
E-mail: rob.cifelli@noaa.gov

DOI: 10.1175/2010JTECHA1488.1

1. Introduction

Radar is an important tool for rainfall estimation because of the relatively high spatial and temporal sampling and ability to cover a relatively large area (>30 000 km^2 for a range of 100 km; see Bringi and Chandrasekar 2001). However, as pointed out by Wilson and Brandes (1979), Austin (1987), Joss and Waldvogel (1990), and many others, radar precipitation estimates are plagued by a number of uncertainties, including calibration of the radar system, partial beam filling, attenuation of the radar signal, contamination resulting from the brightband signature from the melting layer, the fact that rainfall at the ground is estimated from measurements aloft, and variability resulting from radar measurements collected over sampling volumes many orders of magnitude greater than point measurements (rain gauges) on the ground. Rainfall estimation with radar has traditionally been accomplished by relating the backscattered power (converted to the copolar reflectivity factor Z_h) to rainfall through a so-called Z–R relation [hereafter $R(Z_h)$]. It can be shown theoretically that this $R(Z_h)$ relation is not unique and depends on the drop size distribution (DSD), which can vary both from storm to storm and within the storm itself. Variability in the DSD provides another source of uncertainty in radar rainfall estimation.

Dual-polarization radar systems provide both backscatter and differential propagation phase information and therefore can reveal additional characteristics of the precipitation medium to constrain the uncertainty of rainfall estimation resulting from DSD variability. In addition to Z_h, differential reflectivity (Z_{dr}) and specific differential phase (K_{dp}) are typically used either alone or in combination to estimate rainfall. Because it is immune to absolute radar calibration and partial beam blocking, and can be used to correct for attenuation through heavy precipitation, K_{dp} offers additional advantages (Zrnić and Ryzhkov 1996). The relationships between the polarization observations and rainfall, namely, $R(Z_h)$, $R(Z_h, Z_{dr})$, and $R(K_{dp})$ $R(K_{dp}, Z_{dr})$, have been established primarily through theoretical studies with various assumptions about the parameters of the DSD (see Bringi and Chandrasekar 2001 for a review). Because K_{dp} is a derived quantity (estimated from measurements of differential propagation phase), the choice of the filtering technique contributes to variability in the magnitude of the $R(K_{dp})$ and $R(K_{dp}, Z_{dr})$ estimates.

Studies examining the error structure of dual-polarization rainfall estimators have shown that their efficacy varies as a function of rainfall rate. Chandrasekar and Bringi (1988) studied the error structure of $R(Z_h, Z_{dr})$ and concluded that, in light rain, this relationship did not improve rainfall estimation over $R(Z_h)$. Sachidananda and Zrnić (1987) and Chandrasekar et al. (1990, 1993) have shown that $R(K_{dp})$ is noisy at low rain rates but outperforms $R(Z_h)$ and $R(Z_{dr})$ at high rain rates. Jameson (1991) and Ryzhkov and Zrnić (1995) developed rainfall relationships using K_{dp} and Z_{dr} in combination. The latter study showed that $R(K_{dp}, Z_{dr})$ outperform $R(Z_h)$, $R(Z_h, Z_{dr})$, and $R(K_{dp})$ at moderate to heavy rain rates, although the smoothing of K_{dp} and Z_{dr} were necessary to achieve the improved accuracy over $R(K_{dp})$ alone.

Individual rainfall estimators have been combined into algorithms that select the most appropriate rainfall relation for a given set of dual-polarization characteristics. Investigators have given different names for this combination approach (e.g., ''synthetic,'' ''optimal,'' or ''blended''). In this paper, we refer to any algorithm that utilizes one or more rainfall estimators and selects an individual rainfall estimator depending on the radar-observed characteristics (Z_h, Z_{dr}, K_{dp}) as an optimization rainfall algorithm. Several S-band optimization algorithms have been tailored for estimating precipitation in either individual events or for multiple events occurring in specific geographical regions (Chandrasekar et al. 1993; Petersen et al. 1999; Cifelli et al. 2002, 2003, 2005; Ryzhkov et al. 2005a,b; Giangrande and Ryzhkov 2008). We now briefly describe two optimization algorithms that have addressed ice contamination using dual-polarization measurements for operational rainfall products. One algorithm is similar to the method developed at the National Severe Storms Laboratory (NSSL) during the Joint Polarization Experiment (JPOLE) and the other originated at Colorado State University (CSU)-ICE. These algorithms, which will be used as the basis for the comparison for a new optimization algorithm, are further discussed in section 2.

Our rationale for using the CSU and JPOLE algorithms is as follows: 1) the methodologies are fully described in the literature [for CSU see Cifelli et al. (2002) and Silvestro et al. (2009), and for JPOLE, see Ryzhkov et al. (2005a,b)]; and 2) they are relatively easy to implement. A more sophisticated version of the JPOLE optimization algorithm has been developed (Giangrande and Ryzhkov 2008). However, because of the complexity, it was not included in this analysis. For ranges <100 km, Giangrande and Ryzhkov (2008) show that the revised JPOLE formulation improves the bias but degrades the root-mean-square error (RMSE) relative to the original JPOLE algorithm for an aggregated convective and stratiform dataset.

In this study, we describe a new rainfall algorithm (CSU-HIDRO) developed to address hail contamination in the high plains environment. This algorithm is guided by hydrometeor identification developed exclusively for the rainfall estimation application. Data from three rainfall events in northeast Colorado are used to test the algorithm performance. CSU-HIDRO is not the first algorithm to use hydrometeor identification to guide

rainfall selection (e.g., Cifelli et al. 2005; Giangrande and Ryzhkov 2008); however, the CSU algorithm presented herein is unique in that the hydrometeor identification is developed exclusively for the rainfall application. We compare the results of CSU-HIDRO with the CSU-ICE and JPOLE optimization algorithms as well as the Next Generation Weather Radar (NEXRAD) $R(Z_h)$. Because the JPOLE algorithm has been well documented in the literature, it serves as a reference for comparison to the CSU algorithms. As described below, the implementation of the JPOLE algorithm in this study is referred to as "JPOLE like" because of the fact that negative K_{dp} and negative rain-rate values are not retained, in contrast to the original JPOLE methodology.

Our intent is not to provide an exhaustive evaluation of the different algorithms in all possible rainfall environments. Rather, the purpose is to test the performance of several optimization algorithms on mixed rain and hail events, precipitation that is common in the high plains during the warm season (Dye et al. 1974) and is extremely challenging for radar quantitative precipitation estimation (QPE). We use the cases to contrast the philosophical differences in the rainfall estimation selection process among the optimization algorithms. Although the dataset is by no means comprehensive, it includes sufficient observations to allow us to draw conclusions regarding the way the different algorithms perform in mixed rain and ice situations. It is acknowledged that the results are preliminary and that additional evaluation is necessary.

The paper is organized as follows. Section 2 provides details of the JPOLE and CSU-ICE optimization algorithms and provides the foundation for the new CSU-HIDRO algorithm, which is described in detail in section 3. Section 4 details the Colorado State University–University of Chicago–Illinois State Water Survey (CSU–CHILL) scanning strategy as well as the radar and rain gauges data analysis procedure. In section 5, results of the cases analyzed are described, with particular attention paid to the radar–rain gauges comparisons using the different rainfall estimation procedures. Section 6 summarizes the results and suggests approaches for future research.

2. Description of the JPOLE and CSU-ICE algorithms

The JPOLE algorithm has been described extensively in the literature (Ryzhkov et al. 2005a,b; Giangrande and Ryzhkov 2008), but the CSU-ICE methodology has been discussed only briefly (Cifelli et al. 2003). In the following, we describe important features of both algorithms in order to contrast the methodologies and aid in the interpretation of the results as well as to establish the basis for the description of the new CSU-HIDRO algorithm.

a. JPOLE optimization algorithm

The rain estimation procedures given in Ryzhkov et al. (2005b) were used to calculate dual-polarization radar-based rainfall values according to the JPOLE optimization method. In this method, the magnitude of the rain rate given by the standard Weather Surveillance Radar-1988 Doppler (WSR-88D) $R(Z_h)$ formulation controls the selection of one of three rain-rate expressions. The sequence of equations used is as follows:

(i) Basic $R(Z_h)$ rate-for-rate equation selection using the WSR-88D default parameters (Fulton et al. 1998)

$$R(Z_h) = 0.0170(Z_h^{0.714}), \quad (1)$$

where Z_h is in mm^6 m^{-3} and R is in mm h^{-1}. As per National Weather Service (NWS) procedures, Z_h is limited to the linear scale equivalent of 53 dBZ in an attempt to limit hail contamination.

(ii) Three dual-polarization rate equations based on $R(Z_h)$:

if $R(Z_h) < 6$ mm h^{-1}, then

$$R = R(Z_h)/(0.4 + 5.0|Z_{dr} - 1|^{1.3}); \quad (2)$$

if $6 < R(Z_h) < 50$ mm h^{-1}, then

$$R = R(K_{dp})/(0.4 + 3.5|Z_{dr} - 1|^{1.7}); \quad \text{and} \quad (3)$$

if $R(Z_h) > 50$ mm h^{-1}, then $R = R(K_{dp})$, where

$$R(K_{dp}) = 44.0|K_{dp}|^{0.822}\,\text{sign}(K_{dp}), \quad (4)$$

and where Z_{dr} is a linear scale value and K_{dp} is the one-way differential propagation phase value (° km^{-1}). Similar to Brandes et al. (2001), sensitivity tests showed that the algorithm performance improved (in terms of bias and root-mean-square error) when negative K_{dp} and rain-rate values in Eq. (4) were set to zero. This formulation of the algorithm was therefore adopted for the present study and we hereafter refer to the algorithm as "JPOLE like."

b. CSU-ICE optimization algorithm

As noted above, rainfall in the high plains is frequently mixed with hail/graupel during the summer months. The large amount of ice observed at the ground in the high plains region is primarily due to low relative humidity and subsequent evaporative cooling in the subcloud layer, which offsets the melting process (Rasmussen and Heymsfield 1987). Discussions with forecasters from the NWS in the Denver, Colorado, region revealed that, while large hail

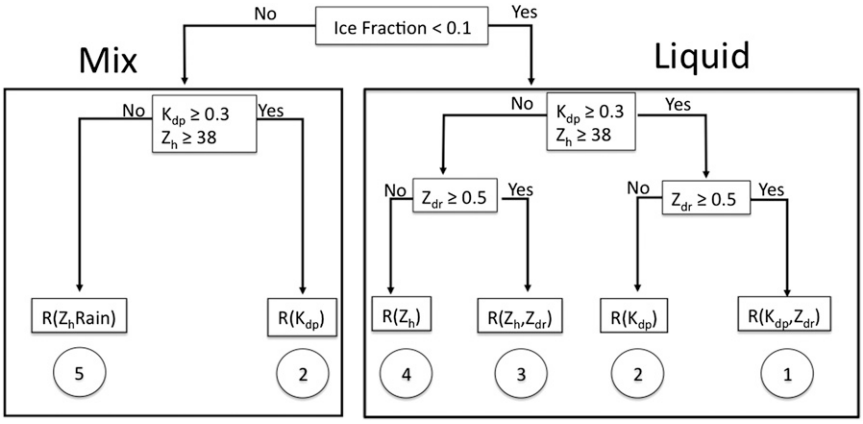

FIG. 1. Flowchart describing the CSU-ICE optimization algorithm logic. The rainfall estimators corresponding to the circled numbers are identified in the text as Eqs. (7)–(11), respectively.

can be identified in WSR-88D radar reflectivity data ($Z_h >$ 60 dBZ), small hail and rainfall mixtures are much more difficult to identify with radar reflectivity alone. Misidentification of rain and precipitation ice often leads to poor rainfall estimation and has important implications for flood forecasting. The challenges of the high plains meteorological environment resulted in the development of an algorithm guided by the precipitation ice fraction in the radar volume. This algorithm is referred to as CSU-ICE.

The CSU-ICE algorithm uses the difference reflectivity (Z_{dp}; Golestani et al. 1989) to estimate the fraction of ice observed in a radar volume. The ice fraction is then used to guide the rainfall estimation method (Fig. 1). The difference reflectivity is defined as

$$Z_{dp} = 10 \log_{10}(Z_h^{rain} - Z_v^{rain}), \quad (5)$$

where Z_h^{rain} and Z_v^{rain} are the linear rain-only reflectivities at horizontal and vertical polarization, respectively. An important assumption is that $Z_h^{ice} \sim Z_v^{ice}$; that is, ice is assumed to scatter isotropically. However, for raindrops larger than about 1 mm the shape becomes an oblate spheroid, such that $Z_h^{rain} > Z_v^{rain}$. Large raindrops backscatter more energy to the radar so that Z_h increases markedly with drop size. A rain line is developed by regressing Z_h against Z_{dp} in precipitation regions that contain rain only. The rain line is then applied in regions where precipitation ice may occur. The difference of the observed Z_h with the value expected for rain only represents the amount of ice in the radar volume according to

$$\text{fi} = 1 - 10^{(-0.1\Delta Z)}, \quad (6)$$

where fi is the ice fraction and ΔZ represents the offset in the observed Z_h and the value expected for Z_h^{rain}. Sensitivity tests show that although the slope and offset of the rain line can vary from storm to storm, the change is small and does not have a pronounced effect on the CSU-ICE algorithm performance. For the CSU-ICE algorithm, the rain line from a high plains mesoscale convective system (MCS) is utilized (Carey and Rutledge 1998).

The rain estimation equations used in the CSU-ICE algorithm (mm h^{-1}) corresponding to the flowchart in Fig. 1 are

$$R(K_{dp}, Z_{dr}) = 90.8(K_{dp})^{0.93} 10^{(-0.169 Z_{dr})} \quad (7)$$

$$R(K_{dp}) = 40.5(K_{dp})^{0.85} \quad (8)$$

$$R(Z_h, Z_{dr}) = 6.7 \times 10^{-3} (Z_h)^{0.927} 10^{(-0.343 Z_{dr})} \quad (9)$$

$$R(Z_h) = 0.0170(Z_h)^{0.7143} \quad (10)$$

$$R(Z_h) = 0.0170(Z_h^{rain})^{0.7143}, \quad (11)$$

where Z_h and Z_h^{rain} are in $mm^6\ m^{-3}$, Z_{dr} is in decibels, and K_{dp} is in degrees per kilometer. Equations (7)–(9) are physically based. The relationships were derived from theoretical considerations assuming a range of gamma DSD parameters that are typically found in observations[1] (see Bringi and Chandrasekar 2001). Equations (7) and (9) assume that drop shape as a function of size follows the Beard and Chuang (1987) equilibrium model, which includes changes resulting from drop oscillations. Equation (10)

[1] As described in chapter 8 of Bringi and Chandrasekar (2001), the gamma DSD parameter ranges are $10^3 \leq N_w \leq 10^5\ mm^{-1}\ m^{-3}$, $0.5 \leq D_0 \leq 2.5$ mm, and $-1 \leq \mu \leq 5$ with $R \leq 300$ mm h^{-1}, where N_w is the normalized intercept parameter, D_0 is the median volume diameter, and μ is the shape parameter.

is the WSR-88D relationship described earlier. Equation (11) is identical to (10), except that the rain-only portion of Z_h (as determined from the ice fraction) is utilized. The CSU-ICE methodology has recently been scaled to C band, and the algorithm demonstrated excellent performance in a wide variety of rainfall regimes (Silvestro et al. 2009).

As shown in Fig. 1, the method of rainfall estimation in the CSU-ICE algorithm is based on thresholds of Z_h, Z_{dr}, and K_{dp} as opposed to rainfall intensity in the JPOLE algorithm. The thresholds were derived from Petersen et al. (1999) by visual inspection of collocated grid points to discriminate signal from noise, and from results reported in Bringi et al. (1996). The latter study quantified the error characteristics of selected polarimetric variables, including Z_h, Z_{dr}, and K_{dp}. The philosophy of rainfall estimation selection in CSU-ICE is to identify situations in which a particular rainfall estimator's performance is maximized. For example, $R(K_{dp}, Z_{dr})$ has the lowest error characteristics in liquid precipitation and is the preferred estimator if both K_{dp} and Z_{dr} are above their respective noise thresholds. If ice is present, then $R(K_{dp})$ is the preferred estimator because Z_{dr} is usually near zero. In situations where K_{dp} and Z_{dr} are noisy or missing $R(Z_h)$ is the fallback position.

Sensitivity tests have shown that the ice fraction discrimination [Eqs. (5) and (6)] in CSU-ICE can produce spurious results in situations where the reflectivity is moderate ($38 < Z_h < 45$). For a given uncertainty in Z_{dr}, the response of Z_{dp} is largest when Z_h^{rain} and Z_v^{rain} are nearly equal (with regions of small nearly spherical drops). This is due to the logarithmic function required in the calculation of Z_{dp} [see (5)]. The result is an apparent offset from the rain line that translates into a spurious large ice fraction. Thus, in light rain situations with $Z_h < 38$ dBZ, the CSU-ICE algorithm will often use method 5 with the Z_h^{rain} as the rainfall estimator (lower-left branch of the flowchart shown in Fig. 1). As ice fraction becomes large, Z_h^{rain} decreases and the resulting rain rate approaches zero. Although light rain does not contribute significantly to the overall rain volume, the resulting rain rates are nevertheless erroneous.

3. CSU-HIDRO optimization algorithm

A new algorithm was developed in order to avoid various problems with rainfall estimates described above and to guide the rainfall estimation selection procedure based on hydrometeor identification (HID) as opposed to ice fraction. This algorithm is referred to as CSU-HIDRO. Previous work by Cifelli et al. (2005) and Giangrande and Ryzhkov (2008) has demonstrated promising results for optimization algorithms driven by HID. A three-class HID was developed specifically for this purpose. Although more classes could be recognized (e.g., Liu and Chandrasekar 1998, 2000; Vivekanandan et al. 1999; Giangrande and Ryzhkov 2008) for the purposes of rainfall estimation, it is necessary only to distinguish the presence of precipitation ice from pure rain. We refer to this three-tier approach as the Hydrometeor Classification System for Rainfall Estimation (HCS-R). The HCS-R utilizes a fuzzy logic approach to guide rainfall estimation. The fuzzy logic technique is well suited for hydrometeor classification resulting from the ability to identify hydrometeor types with overlapping and noise-contaminated measurements. There are several articles in the literature over the last few years describing various aspects of fuzzy logic hydrometeor classification (Vivekanandan et al. 1999; Liu and Chandrasekar 1998; 2000; Zrnić et al. 2001; Lim et al. 2005). A fuzzy logic classification system typically consists of three principal components: 1) fuzzification, 2) inference, and 3) defuzzification. Fuzzification is the process used to convert the precise input measurements to fuzzy sets with a corresponding membership degree. Inference is a rule-based procedure to obtain the strength of individual propositions. Defuzzification is an aggregation of rule strength and a selection of the best representative.

The HCS-R used here is based on the algorithm proposed by Lim et al. (2005). The advantage of this algorithm is to balance the metrics of probability error and false positive classification by using both additive and product rules in inference. The system also uses the weight factor extensively according to hydrometeor types and radar variables. By applying the weight factors for radar variables, we can use the observations more effectively to identify precipitation types, taking their error structure into consideration. In addition, the classifier is separated into two schemes according to the quality of linear depolarization ratio (LDR). The system has been evaluated extensively with S-band CSU–CHILL radar (Lim et al. 2005), the C-band University of Huntsville Advanced Radar for Meteorological and Operational Research (ARMOR) instrument (Baldini et al. 2005), and the C-band University of Helsinki research radar (Keranen et al. 2007).

The architecture of hydrometeor classification proposed here is similar to Lim et al. (2005), except for the output categories. Inputs of HCS-R are five radar observations [Z_h, Z_{dr}, K_{dp}, LDR, and copolar correlation coefficient (ρ_{co}); see Bringi and Chandrasekar (2001) for a detailed description of these parameters] and one environmental variable (temperature T). Outputs of HCS-R are rain, mixture, and ice. Drizzle, moderate rain, and heavy rain are included in the rain category. Mixture includes wet snow and a rain–hail mixture. The ice category includes dry snow, graupel, and hail. Inference and defuzzification process are the same as those in Lim et al. (2005). The general architecture of HCS-R is shown in Fig. 2.

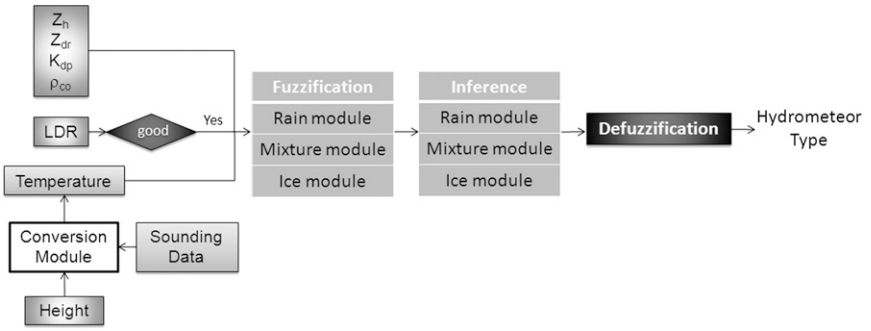

FIG. 2. Flowchart of the HCS-R logic that shows the inputs and steps used to identify hydrometeors.

Once the hydrometeor classification is performed, rainfall estimates can be computed. To compare with rain gauges, the gauge locations within the radar data need to be determined. We use an interpolation procedure described below in section 4. For each rain gauge location, the six nearest radar range gates are identified, and it is required that these six surrounding range gates have valid HIDs (i.e., rain, mixture, or ice); otherwise, no rain-rate estimate is attempted. Although an estimate could be attempted when less than six surrounding range gates have valid HIDs, the preliminary results, described below, indicate good performance of the CSU-HIDRO algorithm with the conservative approach adopted herein. The CSU-HIDRO algorithm assumes that a simple majority of the six surrounding range gates ''wins'' the HID classification of the rain gauges location. In rare situations where there is a ''tie'' of different HID categories (e.g., three range gates are identified as rain and three range gates are identified as mixture), the following procedures are applied:

1) rain–mix tie: a linear average is calculated using the appropriate rainfall estimators for liquid and mixture;
2) rain–ice tie: the appropriate liquid estimator is applied; and
3) mix–ice tie: the appropriate mix estimator is applied.

The logic of CSU-HIDRO is shown as Fig. 3.

4. Data description

a. CSU–CHILL radar data

The CSU–CHILL radar is an S-band dual-polarization system operating at 2.725 GHz, located near Greeley, Colorado. The radar routinely collects a full suite of dual-polarization measurements, including Z_h, Z_{dr}, differential propagation phase (Φ_{dp}), ρ_{hv}, and LDR. For the events reported herein, radar data were collected by operating the CSU–CHILL radar with the transmitted polarization varying between horizontal (H) and vertical (V) on a pulse-to-pulse basis. The individual pulses were 1 μs in duration (150-m-range gate length) with a pulse repetition time (PRT) of 1042 μs. Digital processing of the received signals included the application of a clutter filter. The antenna azimuthal scan rate was nominally 6° s^{-1}, and data rays were output at azimuth intervals of ~0.75°.

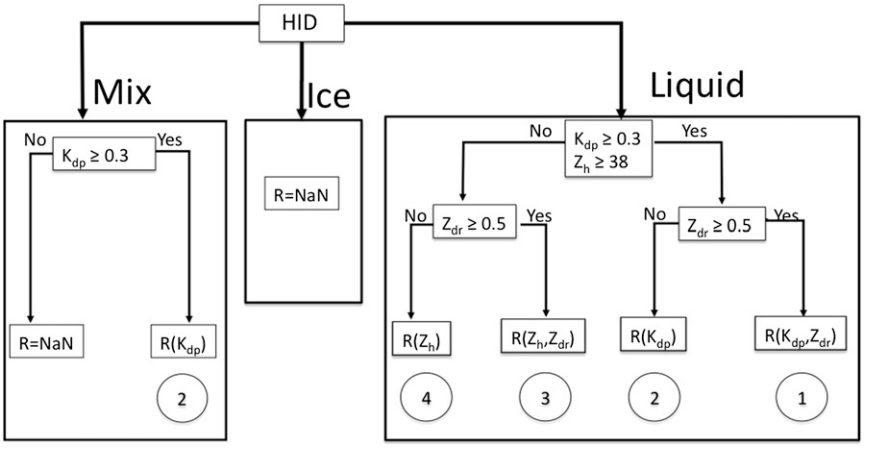

FIG. 3. Flowchart describing the CSU-HIDRO algorithm logic. The rainfall estimators corresponding to the circled numbers are the same as in Fig. 1 and are described in the text.

TABLE 1. Summary of observations for the three precipitation events. Columns (from left to right) refer to the date and time (UTC) of CSU–CHILL radar observations, number of rain gauges used in the analysis, mean gauge accumulation, maximum gauge accumulation, the update time of the CSU–CHILL radar scans, and notes regarding the precipitation type or intensity. DEN refers to Denver.

Date	Time (UTC)	No. of gauges	Mean gauge accumulation (mm)	Max gauge accumulation (mm)	CSU–CHILL radar sweep cycle time (min)	Remarks
9–10 Jun 2005	2227–0101	17	8.2	22.9	1:10	Rain + small hail
19–20 Aug 2006	2242–0113	12	15.7	26.9	1:15	Local DEN street flooding
9 Aug 2008	0102–0320	18	29.1	75.9	3:17	Flash flooding in southeast DEN

Additional technical information on the CSU–CHILL radar is available online (see http://chill.colostate.edu/).

The radar system was calibrated using a series of standard measurements made on each day of meteorological data collection, which included solar, transmitter, and receiver calibrations. These calibration procedures kept the reflectivity uncertainty to $\sim\pm1.5$ dB. Similarly, several procedures were used to calibrate the radar's Z_{dr} measurements. Through these combined efforts, it is believed that uncertainty in the individual range gate Z_{dr} values is $\sim\pm0.15$ dB.

Because of the rapid fluctuations that occur in convective precipitation, the radar was scanned so that a $\sim0.5°$ elevation angle plan position indicator (PPI) pass was made over rain gauges network at time intervals of 3 min or less (see Table 1 for the scan specifics of each precipitation event). Nonmeteorological echoes were removed from the data using thresholds on correlation coefficient (0.9) and differential propagation phase variability (0.98) as described in Wang and Chandrasekar (2009).

An interpolation procedure based on the methods of Mohr and Vaughan (1979) was developed to provide radar data values derived from the lowest elevation angle PPI sweep over selected rain gauge locations. This process began with the identification of the two data rays whose azimuths flanked the gauge location. The number of the radar gate with an Earth-projected range that most nearly matched that of the gauge was also determined. Based on this central gate number, data from six contributing radar sample points (i.e., the central gate plus or minus one gate in each of the two flanking rays) were available. The interpolation process began with the calculation of triangle-weighted range averages for each data field (Z_h, Z_{dr}, and K_{dp}) in the two flanking rays. These range-averaged results were then interpolated with respect to azimuth angle to develop radar data values appropriate for the gauge's angular location between the two flanking rays (Fig. 4). Quality control on the interpolation input data was obtained using a data mask field that objectively identified gates where meteorological echoes (versus noise, ground clutter, etc.) were present. The interpolation results were only considered to be valid when the radar data mask identified meteorological returns in all six of the contributing gates.

The Z_h, Z_{dr}, and K_{dp} values interpolated to the rain gauges locations were used as inputs for the CSU-ICE, CSU-HIDRO, and JPOLE-like optimization algorithms. For consistency, the K_{dp} values input to the JPOLE-like rainfall algorithm were computed using JPOLE procedures. Following Ryzhkov et al. (2005a), the steps used in these JPOLE K_{dp} values were as follows:

1) A running five-gate median filter was applied to the basic Φ_{dp} data in each ray.
2) A ρ_{hv} threshold of 0.85 was used to remove nonmeteorological sections from the filtered Φ_{dp} data.
3) The K_{dp} values were obtained from the slope of the linear best-fit line derived from 9-gate (''lightly filtered'' K_{dp}) and 25-gate (''heavily filtered'' K_{dp}) segments of the filtered Φ_{dp} data.
4) Linear interpolation was used to fill in gaps in the lightly and heavily filtered rays of the K_{dp} data. (These

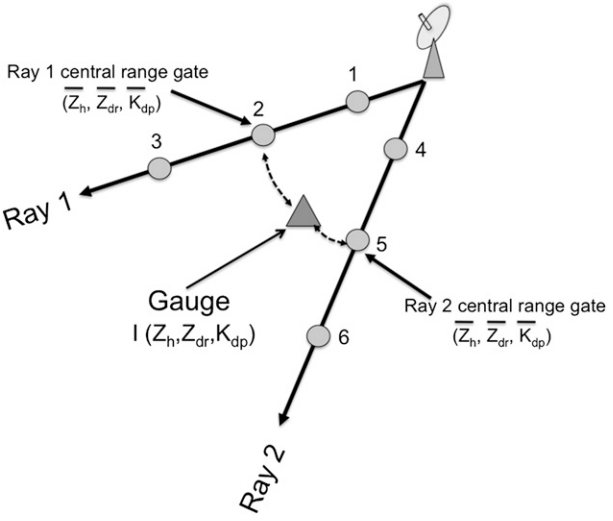

FIG. 4. Schematic illustration of the interpolation methodology used in the analysis, as described in the text. The I (Z_h, Z_{dr}, K_{dp}) refers to the interpolated values of horizontal reflectivity (dBZ), differential reflectivity (dB), and specific differential phase ($° \text{ km}^{-1}$) at the gauge location.

filled-in K_{dp} regions were generally outside of precipitation areas and played virtually no role in the rainfall calculations.)

The resultant rays of the lightly and heavily filtered K_{dp} gate data values were interpolated to the rain gauges locations using the previously described flanking ray method. As per JPOLE procedures, the K_{dp} selection was made based on the interpolated reflectivity level: the heavily filtered K_{dp} was used for reflectivities below 40 dBZ and the lightly filtered K_{dp} was used when reflectivities reached or exceeded 40 dBZ.

CSU–CHILL data collected from three fairly intense convective precipitation events over the Denver area rain gauge network were processed to determine rain rates for each optimization algorithm. Integration of the resultant rain rates over the time steps between the 0.5° elevation angle PPI sweeps were used to develop rain accumulations.

b. Rain gauge data

It is well known that radar–gauge comparisons are complicated because of a combination of differences in sampling geometry, DSD, subcloud drop evaporation or coalescence/breakup, advection of drops in or out of the gauge line of sight, and temporal sampling (Harrold et al. 1974; Wilson and Brandes 1979; Zawadzki 1984; Joss and Waldvogel 1990; Kitchen and Jackson 1993; Fabry et al. 1994; Joss and Lee 1995, and many others). It is also recognized that tipping-bucket gauges tend to underestimate rainfall in windy conditions (Sevruk 1996). However, the gauges do provide a baseline for comparison with the radar estimates. In this study, the emphasis is on the relative performance of each optimization algorithm as opposed to achieving perfect agreement with the gauges.

Rain gauge data for this study were obtained from the Urban District Flood and Drainage (UDFCD) Automated Local Evaluation in Real Time (ALERT) network in Denver. There are over 100 automated tipping-bucket gauges in this network supplying data in near–real time. The time of each tip as well as the running accumulation is sent via telemetry to a computer server. The tip resolution of the UDFCD gauges is 1 mm. Accumulation time series files were extracted from a subset of the UDFCD gauges (12–18 in total) that contained at least 3 mm of precipitation for the event in question and were covered by the CSU–CHILL radar. This selection process ensured that the optimization algorithms were exercised primarily in heavy rain and hail situations. The gauges were approximately 70–90 km from the CSU–CHILL radar, yielding a nominal beam height of about 1 km AGL (for an elevation angle of 0.5°). To ensure that the radar–rain gauges comparisons only included rainfall during the periods of radar coverage, the rain gauge accumulations were restricted to the start and end time (plus 10 min) of radar coverage over the UDFCD network for each event. The additional 10 min at the end of radar operations were included to account for fall time and advection of rain between the cloud and ground.

TABLE 2. Results for the 9 Jun 2005 event.

Radar algorithm	RMSE (mm)	NB (%)	CORR
CSU-ICE	4.1	8.4	0.60
CSU-HIDRO	4.8	−6.5	0.40
JPOLE-like	6.6	33.4	0.24
NEXRAD $R(Z_h)$	10.8	83.1	0.49
$R(K_{dp})$	4.3	−6.6	0.52
$R(K_{dp}, Z_{dr})$	5.4	33.5	0.58
$R(Z_h, Z_{dr})$	51.9	435	0.50

Rainfall accumulations over the duration of each event (≥2 h) are used to compare the relative performance of each optimization algorithm. For each event, statistics of the RMSE, normalized bias (NB), and the Pearson correlation coefficient (CORR) were obtained as indications of each algorithm's performance,

$$\mathrm{RMSE} = \left[\frac{1}{N}\sum_{i=1}^{N}(\mathrm{RA}_i^{\mathrm{radar}} - \mathrm{RA}_i^{\mathrm{gauge}})^2\right]^{1/2},$$

$$\mathrm{NB} = \left(\frac{\overline{\mathrm{R}}\,\overline{\mathrm{A}}^{\mathrm{radar}} - \overline{\mathrm{R}}\,\overline{\mathrm{A}}^{\mathrm{gauge}}}{\overline{\mathrm{R}}\,\overline{\mathrm{A}}^{\mathrm{gauge}}}\right) \times 100,$$

$$\mathrm{CORR} = \frac{\mathrm{covar}(\mathrm{RA}^{\mathrm{radar}}, \mathrm{RA}^{\mathrm{gauge}})}{\sigma^{\mathrm{gauge}}, \sigma^{\mathrm{radar}}},$$

where RA represents accumulation from either a gauge or radar, σ is standard deviation in millimeters, RMSE is in millimeters, NB is in percent, CORR is dimensionless, and the overbar represents mean values.

5. Results

An overview of the three events is presented in Table 1. Precipitation during each event was intense with maximum rain accumulations in the UDFCD network ranging from ~23 to 76 mm during the approximate 2.5 h of sampling. There were local reports of rain mixed with hail (9–10 June 2005) and flooding (19–20 August 2006 and 9 August 2008).

The following presents a summary of the performance of the CSU-ICE, CSU-HIDRO, and JPOLE-like optimization algorithms and compares the results to the NEXRAD $R(Z_h)$ method. RMSE, NB, and CORR results for each of the events, as well as for all cases combined, are shown in Tables 2–5. We also show scatterplots of the radar–gauge comparisons for the three cases combined in Fig. 5 (scatterplots of the individual events are not shown

TABLE 3. Results for the 19 Aug 2006 event.

Radar algorithm	RMSE (mm)	NB (%)	CORR
CSU-ICE	4.3	10.5	0.80
CSU-HIDRO	4.0	17.7	0.91
JPOLE-like	11.0	64.5	0.82
NEXRAD $R(Z_h)$	6.8	19.8	0.64
$R(K_{dp})$	4.1	−0.59	0.68
$R(K_{dp}, Z_{dr})$	5.0	21.6	0.83
$R(Z_h, Z_{dr})$	11.0	48.4	0.78

TABLE 4. Results for the 9 Aug 2008 event.

Radar algorithm	RMSE (mm)	NB (%)	CORR
CSU-ICE	11.1	10.5	0.83
CSU-HIDRO	11.2	8.2	0.82
JPOLE-like	14.3	22.1	0.76
NEXRAD $R(Z_h)$	28.3	80.6	0.71
$R(K_{dp})$	11.3	12.1	0.83
$R(K_{dp}, Z_{dr})$	9.9	4.2	0.86
$R(Z_h, Z_{dr})$	25.1	68.4	0.87

because they show essentially the same results as those in Fig. 5). Tables 2–4 indicate that all of the optimization algorithms display a positive bias relative to the rain gauges for the three cases with the exception of the CSU-HIDRO in the 9 June 2005 event. The NEXRAD algorithm nearly always shows the largest positive bias, which is evident in the combined scatterplot (Fig. 5). The large positive bias is due to the inability of the $R(Z_h)$ algorithm to discriminate between mixtures of heavy rain and precipitation ice. In situations where graupel and/or hail are present, the NEXRAD algorithm assumes that these ice hydrometeors are large raindrops and produces high-intensity rain rates (Fig. 6). Even with a maximum threshold of 53 dBZ, the NEXRAD $R(Z_h)$ often produces rain rates that are far in excess of both the gauge and optimization algorithm estimates. In contrast, the optimization algorithms take advantage of the differential phase and differential reflectivity information to estimate rainfall and they are usually in much better agreement with the rain gauge.

Both the CSU-ICE and CSU-HIDRO algorithms perform similarly in terms of bias and error, with NB values <20% and RMSE <12 mm (Tables 2–5). The estimates from the CSU algorithms were also generally well correlated with the rain gauge results, with correlation coefficients ranging from 0.8 to 0.91 for the August 2006 and 2008 events (Tables 3–4). Correlation coefficients were lower in the June 2005 event (Table 2), likely resulting from the significant amount of hail reported in this event. Overall, the agreement is excellent, especially considering that the gauges are 70–90 km from the CSU–CHILL radar. We note that the $R(K_{dp}, Z_{dr})$ and $R(K_{dp})$ estimators in Eqs. (7)–(8) performed similarly to those in CSU-ICE and CSU-HIDRO in each event (Tables 2–5). This was likely due to the selection of rain gauges that was used (see the description in section 4b), which emphasized heavy rain and ice where K_{dp} is known to provide superior estimation of rainfall. The JPOLE-like algorithm bias is larger than the CSU results, but is still generally better than those from NEXRAD $R(Z_h)$ (Tables 2–5). The larger uncertainty in the JPOLE-like estimates compared to those from CSU is probably due to the combined effects of different DSDs in northern Colorado compared to Oklahoma, the threshold of ice contamination, and the method used to calculate K_{dp}. However, a detailed error analysis documenting the various factors influencing the JPOLE-like algorithm is beyond the scope of this paper.

The different guides for the CSU and JPOLE-like optimization algorithms (i.e., ice fraction and HID for CSU or Z_h for JPOLE-like) translate into differences in the rainfall estimator that is used most frequently and contributes more to the total rain volume. As shown in Fig. 7, the JPOLE-like algorithm utilizes $R(Z_h, Z_{dr})$ most often, while the CSU algorithms mostly utilize $R(Z_h)$ or $R(Z_h^{rain})$, followed closely by $R(Z_h, Z_{dr})$. Recall that in the JPOLE-like formulation, there is no $R(Z_h)$ estimator. In light rain situations, the JPOLE-like algorithm uses $R(Z_h, Z_{dr})$ as in (2), while the CSU algorithms use $R(Z_h)$ from (10). Although often utilized, these estimators contribute <10% of the total rain volume (Fig. 7b). The frequent occurrence of these estimators reflects the fact that, over the gauges most of the time, the storm intensity is relatively weak with low K_{dp} and Z_h values. In these situations, the $R(K_{dp})$ estimators are used much less frequently in all of the optimization algorithms. Although the JPOLE-like algorithm selects $R(K_{dp})$ <15% of the time, this estimator produces over 40% of the rain volume (Fig. 7b), emphasizing that the large infrequent rains produce the bulk of the rainfall in these events. The rain volume fraction for the CSU algorithms is dominated by $R(K_{dp}, Z_{dr})$ (~60%) and, to a lesser extent, $R(Z_h, Z_{dr})$ (~20%); $R(K_{dp})$ contributes

TABLE 5. Results for all of the events combined.

Radar algorithm	RMSE (mm)	NB (%)	CORR
CSU-ICE	7.7	10.2	0.88
CSU-HIDRO	7.9	8.2	0.87
JPOLE-like	11.3	33.3	0.82
NEXRAD $R(Z_h)$	19.2	67.3	0.79
$R(K_{dp})$	7.8	6.5	0.87
$R(K_{dp}, Z_{dr})$	7.4	12.4	0.89
$R(Z_h, Z_{dr})$	34.4	118	0.55

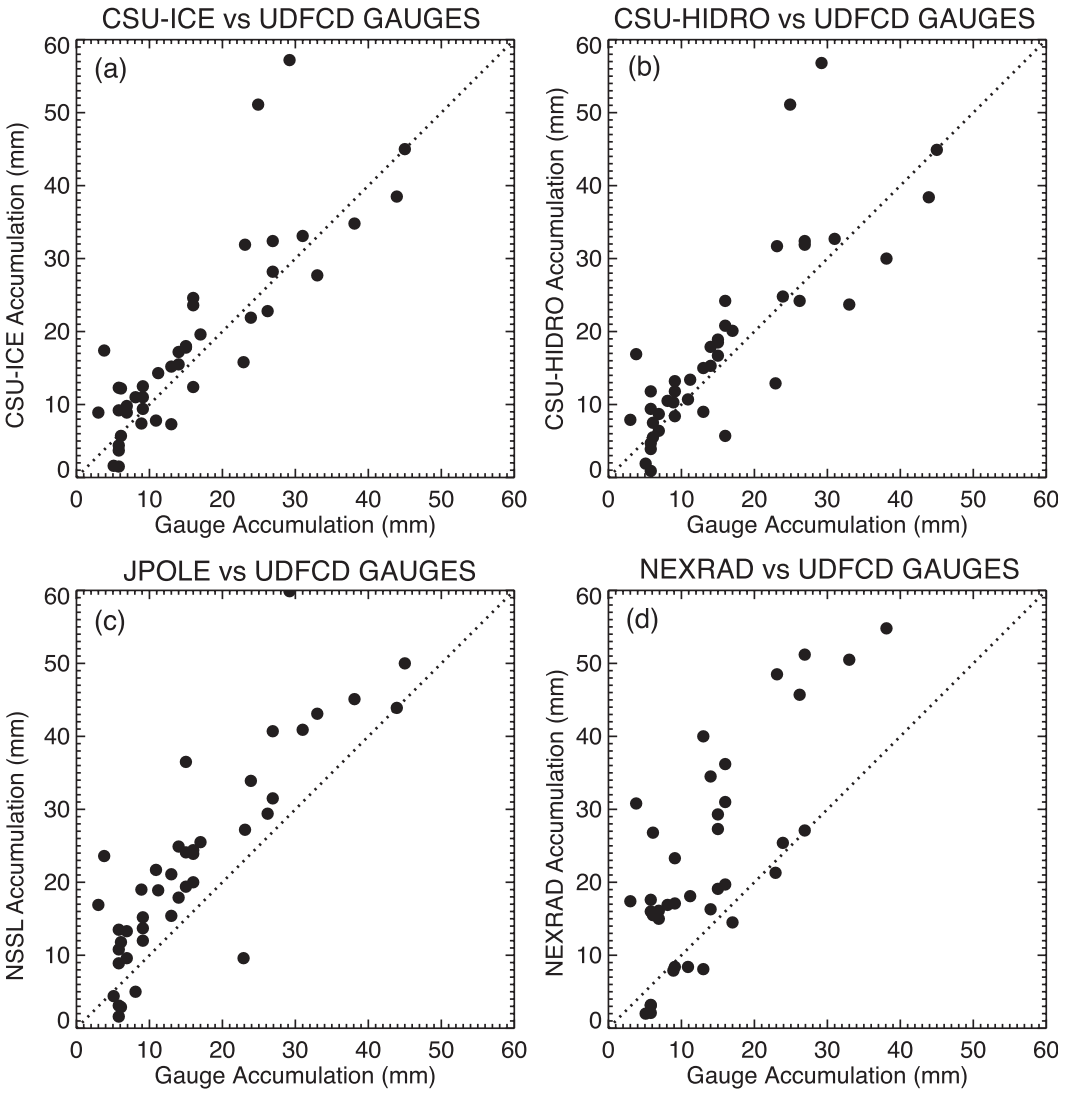

FIG. 5. Scatterplots of radar vs rain gauge accumulation (mm) for all events combined. (a) CSU-ICE, (b) CSU-HIDRO, (c) JPOLE-like, and (d) NEXRAD $R(Z_h)$.

only a small fraction to the total rain volume in both CSU-ICE and CSU-HIDRO.

The higher contribution of $R(K_{dp}, Z_{dr})$ and $R(Z_h, Z_{dr})$ to rain volume in the CSU methods compared to the JPOLE-like method reflects the difference in philosophy in rainfall estimator selection between the optimization algorithms. For the JPOLE-like technique, the rainfall selection is guided by the rain rate estimated by the NEXRAD $R(Z_h)$ [recall Eq. (1)]. For rain rates over 50 mm h^{-1} (equivalent to a Z_h value of ~49 dBZ), it is assumed that $R(K_{dp})$ is the best estimator, independent of the value of Z_{dr}. This is equivalent to assuming that the radar volume may be ice contaminated. In contrast, the CSU algorithms use either ice fraction (CSU-ICE) or HID (CSU-HIDRO) to determine the presence of ice. If ice is not detected, the CSU algorithms can select from a choice of estimators, depending on the characteristics of Z_h, Z_{dr}, and K_{dp}. In other words, there is no a priori assumption in the CSU algorithms that rain rates over 50 mm h^{-1} ($Z_h > 49$ dBZ) indicate ice contamination. We note that the subsequent version of the JPOLE method (Giangrande and Ryzhkov 2008) also uses HID to guide the rainfall estimation and makes greater use of Z_{dr} compared to the original JPOLE formulation.

To better understand the differences between the JPOLE-like and CSU-ICE/CSU-HIDRO methods at high rain rates, it was of interest to determine how often the CSU algorithms did *not* detect the presence of significant ice contamination when the $R(Z_h)$ in (1) indicated rain rates > 50 mm h^{-1}. It was found that, for the events examined herein, the CSU algorithms selected $R(K_{dp}, Z_{dr})$ or $R(Z_h, Z_{dr})$ in approximately 18%–23% of

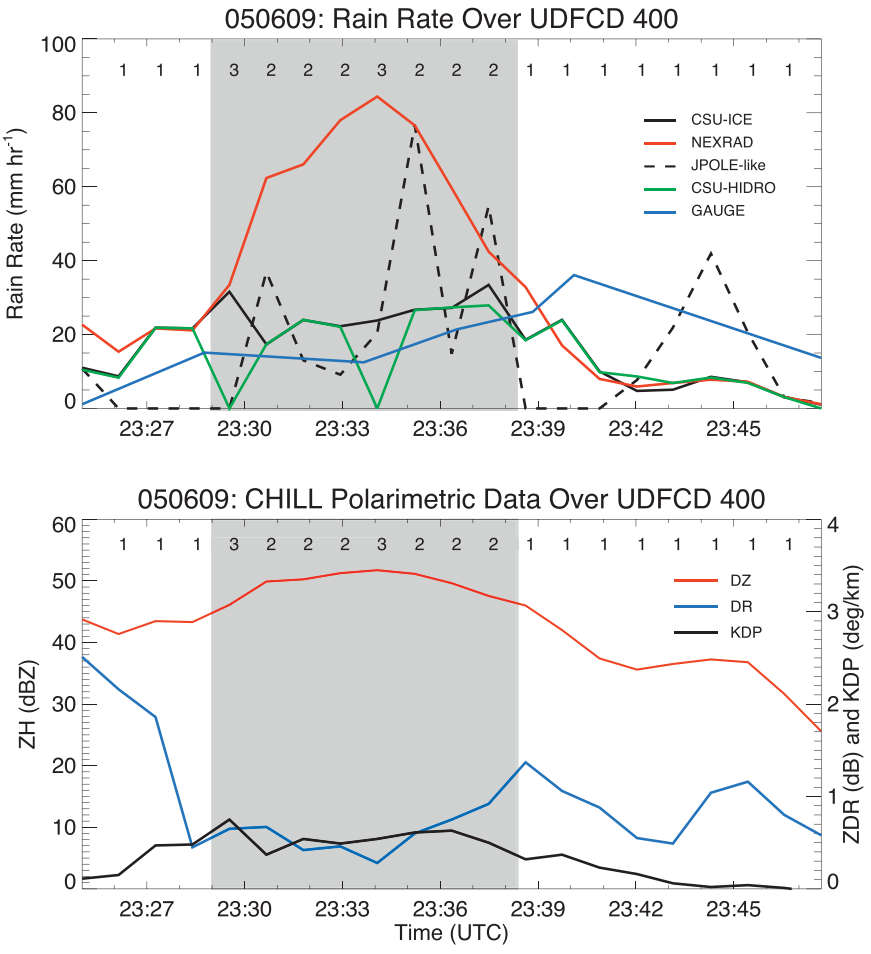

FIG. 6. Time series of (top) rain rate and (bottom) CSU–CHILL radar polarimetric parameters over rain gauge 400 during the 9 Jun 2005 event. Numbers at the top of each plot indicate the HID consensus values: 1) rain, 2) mix, and 3) ice as identified by HCS-R. The shaded region indicates time periods when HCS-R identified the presence of ice. During these time periods, radar reflectivity (Z_h) is relatively large, and differential reflectivity (Z_{dr}) is low. The legend in the top plot indicates the different rainfall algorithms and rain gauge results. Specific differential phase in the bottom plot is the CSU estimate using the Wang and Chandrasekar (2009) methodology.

the situations, while the JPOLE-like algorithm selected $R(K_{dp})$ (not shown). In other words, the CSU algorithms did not detect the presence of ice and utilized the Z_{dr} information in a small *but not negligible* fraction of samples over the rain gauge network. It appears that, at least for the limited set of cases examined, the additional information about the presence/absence of ice in the CSU-ICE and CSU-HIDRO algorithms aided in the reduction of the uncertainty in the radar rainfall estimates.

6. Discussion and conclusions

Dual-polarization radar offers a number of advantages over traditional single-polarization systems. These advantages can be broadly separated into basic and applied science categories. In terms of basic science, dual polarization provides more accurate physical models to represent the DSD and their relationship to the observed radar variables. These radar systems also provide measurements that are immune to absolute radar calibration and partial beam blocking (applied science issues). Dual-polarization observations can be integrated into all three steps of the QPE process to improve rainfall estimation: preprocessing (data enhancement), classification (identification of different hydrometeor types), and quantification (rainfall estimation). By combining the different radar measurements, dual-polarization algorithms have been developed that take advantage of the strengths of different rainfall estimators in different precipitation environments.

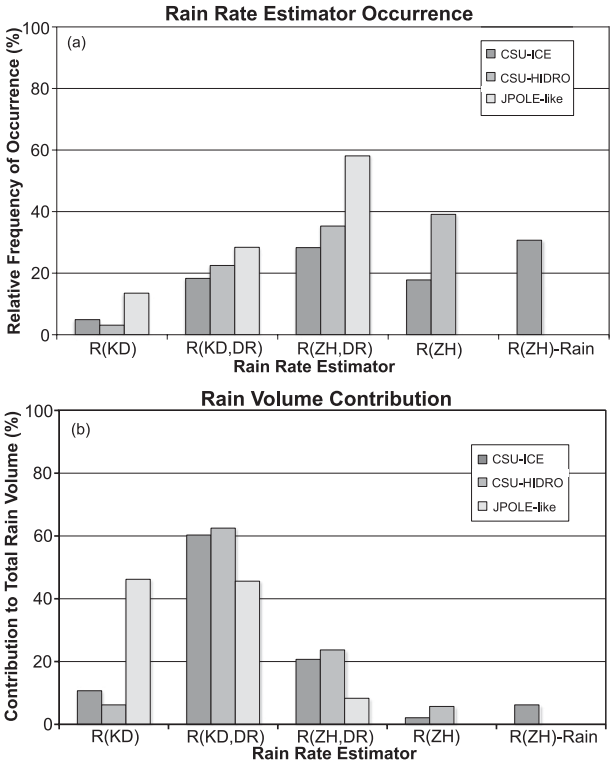

FIG. 7. (a) Relative frequency of occurrence (%) of the different rainfall estimator methods for CSU-ICE, CSU-HIDRO, and the JPOLE-like optimization algorithms from all events combined. (b) As in (a), but for the relative contribution (%) of the different rainfall estimators to total rain volume.

Rainfall estimation using radars in the high plains is always challenging because of ice contamination. In principle, the introduction of dual polarization was expected to help in this situation, but preliminary results from this study suggest that numerous details are important. It has taken significant research to implement these details and see results operationally, such as in JPOLE and the data shown in this paper.

The results of this study indicate that the rainfall accumulations generated by processing dual-polarization radar data using the CSU-HIDRO methodology have a low (~8%) normalized bias and RMSE (~8 mm) when tested against verification data obtained from the passage of three heavy rain and hail events over a rain gauge network. This performance was due to the development of a hydrometeor classification system (HCS-R) optimized for guiding the rain-rate equation selection process as well as improvements made in the estimation of K_{dp}. Based on these initial results, it appears that the CSU-HIDRO algorithm is delivering encouraging results in the high plains environment where ice contamination often complicates radar estimation of rainfall. Further studies are necessary to evaluate the relative performance of the JPOLE-like and CSU algorithms in different precipitation environments.

Acknowledgments. This work was supported by the NASA Precipitation Measurement Mission (PMM) Award NNX09AG49G and the National Science Foundation (NSF) under the CSU–CHILL award ATM 0735110. Kevin Stewart of the Denver Urban Drainage and Flood Control District provided assistance with the rain gauge data. The authors thank Scott Giangrande and two anonymous reviewers for their constructive comments on the manuscript.

REFERENCES

Austin, P. M., 1987: Relation between measured radar reflectivity and surface rainfall. *Mon. Wea. Rev.,* **115,** 1053–1070.

Baldini, L., E. Gorgucci, V. Chandrasekar, and W. Peterson, 2005: Implementations of CSU hydrometeor classification scheme for C-band polarimetric radars. Preprints, *32nd Conf. on Radar Meteorology,* Albuquerque, NM, Amer. Meteor. Soc., P11R.4. [Available online at http://ams.confex.com/ams/pdfpapers/95865.pdf.]

Beard, K. V., and C. Chuang, 1987: A new model for the equilibrium shape of raindrops. *J. Atmos. Sci.,* **44,** 1509–1524.

Brandes, E. A., A. V. Ryzhkov, and D. S. Zrnić, 2001: An evaluation of radar rainfall estimates from specific differential phase. *J. Atmos. Oceanic Technol.,* **18,** 363–375.

Bringi, V. N., and V. Chandrasekar, 2001: *Polarimetric Doppler Weather Radar: Principles and Applications*. Cambridge University Press, 635 pp.

——, L. Liu, P. C. Kennedy, V. Chandrasekar, and S. A. Rutledge, 1996: Dual multiparameter radar observations of intense convective storms: The 24 June 1992 case study. *Meteor. Atmos. Phys.,* **59,** 3–31.

Carey, L. D., and S. A. Rutledge, 1998: Electrical and multiparameter radar observations of a severe hailstorm. *J. Geophys. Res.,* **103,** 13 979–14 000.

Chandrasekar, V., and V. N. Bringi, 1988: Error structure of multiparameter radar and surface measurements of rainfall. Part I: Differential reflectivity. *J. Atmos. Oceanic Technol.,* **5,** 783–795.

——, V. Bringi, N. Balakrishnan, and D. S. Zrnić, 1990: Error structure of multiparameter radar and surface measurements of rainfall. Part III: Specific differential phase. *J. Atmos. Oceanic Technol.,* **7,** 621–629.

——, E. Gorgucci, and G. Scarchilli, 1993: Optimization of multiparameter radar estimates of rainfall. *J. Appl. Meteor.,* **32,** 1288–1293.

Cifelli, R., W. A. Petersen, L. D. Carey, and S. A. Rutledge, 2002: Radar observations of the kinematic, microphysical, and precipitation characteristics of two MCSs in TRMM LBA. *J. Geophys. Res.,* **107,** 8077, doi:10.1029/2000JD000264.

——, and Coauthors, 2003: Evaluation of an operational polarimetric rainfall algorithm. Preprints, *31st Int. Conf. on Radar Meteor.,* Seattle, WA, Amer. Meteor. Soc., P2B.14. [Available online at http://ams.confex.com/ams/pdfpapers/63992.pdf.]

——, P. C. Kennedy, V. Chandrasekar, S. Nesbitt, S. A. Rutledge, and L. Carey, 2005: Polarimetric rainfall retrievals using blended algorithms. Preprints, *32nd Conf. on Radar Meteorology,* Albuquerque, NM, Amer. Meteor. Soc., 9R.1. [Available online at

http://ams.confex.com/ams/32Rad11Meso/techprogram/paper_96556.htm.]

Dye, J. E., C. A. Knight, V. Toutenhoofd, and T. W. Cannon, 1974: The mechanism of precipitation formation in northeastern Colorado Cumulus III. Coordinated microphysical and radar observations and summary. *J. Atmos. Sci.,* **31,** 2152–2159.

Fabry, F., A. Bellon, M. R. Duncan, and G. L. Austin, 1994: High-resolution rainfall measurements by radar for very small basins: The sampling problem revisited. *J. Hydrol.,* **161,** 415–428.

Fulton, R. A., J. P. Breidenbach, D. J. Seo, D. A. Miller, and T. O'Bannon, 1998: The WSR-88D rainfall algorithm. *Wea. Forecasting,* **13,** 377–395.

Giangrande, S. E., and A. V. Ryzhkov, 2008: Estimation of rainfall based on the results of polarimetric echo classification. *J. Appl. Meteor. Climatol.,* **47,** 2445–2462; Corrigendum, **48,** 690.

Golestani, Y., V. Chandrasekar, and V. N. Bringi, 1989: Intercomparison of multiparameter radar measurements. *Proc. 24th Conf. on Radar Meteorology,* Boston, MA, Amer. Meteor. Soc., 309–314.

Harrold, T. W., E. J. English, and C. A. Nicholass, 1974: The accuracy of radar-derived rainfall measurements in hilly terrain. *Quart. J. Roy. Meteor. Soc.,* **100,** 331–350.

Jameson, A. R., 1991: A comparison of microwave techniques for measuring rainfall. *J. Appl. Meteor.,* **30,** 32–54.

Joss, J., and A. Waldvogel, 1990: Precipitation measurement and hydrology. *Radar in Meteorology,* D. Atlas, Ed., Amer. Meteor. Soc., 577–606.

——, and R. Lee, 1995: The application of radar–gauge comparisons to operational precipitation profile corrections. *J. Appl. Meteor.,* **34,** 2612–2630.

Keranen, R., E. Saltikoff, V. Chandrasekar, S. Lim, J. Holmes, and J. Selzler, 2007: Real-time hydrometeor classification for the operational forecasting environment. Preprints, *33rd Conf. on Radar Meteorology,* Cairns, QLD, Australia, Amer. Meteor. Soc., P11B.11. [Available online at http://ams.confex.com/ams/pdfpapers/123476.pdf.]

Kitchen, M., and P. M. Jackson, 1993: Weather radar performance at long range—Simulated and observed. *J. Appl. Meteor.,* **32,** 975–985.

Lim, S., V. Chandrasekar, and V. N. Bringi, 2005: Hydrometeor classification system using dual-polarization radar measurements: Model improvements and in situ verification. *IEEE Trans. Geosci. Remote Sens.,* **43,** 792–801.

Liu, H., and V. Chandrasekar, 1998: Classification of hydrometeor type based on multiparameter radar measurements. Preprints, *Int. Conf. on Cloud Physics,* Everett, WA, Amer. Meteor. Soc., 253–256.

——, and ——, 2000: Classification of hydrometeor based on polarimetric radar measurements: Development of fuzzy logic and neuro-fuzzy systems, and in situ verification. *J. Atmos. Oceanic Technol.,* **17,** 140–164.

Mohr, C. G., and R. L. Vaughan, 1979: An economical procedure for Cartesian interpolation and display of reflectivity factor data in three-dimensional space. *J. Appl. Meteor.,* **18,** 661–670.

Petersen, W. A., and Coauthors, 1999: Mesoscale and radar observations of the Fort Collins flash flood of 28 July 1997. *Bull. Amer. Meteor. Soc.,* **80,** 191–216.

Rasmussen, R. M., and A. J. Heymsfield, 1987: Melting and shedding of graupel and hail. Part II: Sensitivity study. *J. Atmos. Sci.,* **44,** 2764–2782.

Ryzhkov, A., and D. Zrnić, 1995: Precipitation and attenuation measurements at a 10-cm wavelength. *J. Appl. Meteor.,* **34,** 2121–2134.

——, S. E. Giangrande, and T. J. Schuur, 2005a: Rainfall estimation with a polarimetric prototype of WSR-88D. *J. Appl. Meteor.,* **44,** 502–515.

——, T. J. Schuur, D. W. Burgess, P. L. Heinselman, S. E. Giangrande, and D. S. Zrnić, 2005b: The Joint Polarization Experiment: Polarimetric rainfall measurements and hydrometeor classification. *Bull. Amer. Meteor. Soc.,* **86,** 809–824.

Sachidananda, M., and D. S. Zrnić, 1987: Rain-rate estimates from differential polarization measurements. *J. Atmos. Oceanic Technol.,* **4,** 588–598.

Sevruk, B., 1996: Adjustment of tipping-bucket precipitation gauge measurements. *Atmos. Res.,* **42,** 237–246.

Silvestro, F., N. Rebora, and L. Ferraris, 2009: An algorithm for real-time rainfall rate estimation by using polarimetric radar: RIME. *J. Hydrometeor.,* **10,** 227–240.

Vivekanandan, J., S. M. Ellis, R. Oye, D. S. Zrnić, A. Ryzhkov, and J. M. Straka, 1999: Cloud microphysics retrieval using S-band dual-polarization radar measurements. *Bull. Amer. Meteor. Soc.,* **80,** 381–388.

Wang, Y., and V. Chandrasekar, 2009: Algorithm for estimation of the specific differential phase. *J. Atmos. Oceanic Technol.,* **26,** 2565–2578.

Wilson, J. W., and E. A. Brandes, 1979: Radar measurement of rainfall—A summary. *Bull. Amer. Meteor. Soc.,* **60,** 1048–1058.

Zawadzki, I., 1984: Factors affecting the precision of radar measurements of rain. Preprints, *22nd Conf. on Radar Meteorology,* Zurich, Switzerland, Amer. Meteor. Soc., 251–256.

Zrnić, D. S., and A. Ryzhkov, 1996: Advantages of rain measurements using specific differential phase. *J. Atmos. Oceanic Technol.,* **13,** 454–464.

——, ——, J. Straka, Y. Liu, and J. Vivekanandan, 2001: Testing a procedure for automatic classification of hydrometeor types. *J. Atmos. Oceanic Technol.,* **18,** 892–913.